Published in final edited form as:
Biochemistry. 2012 August 28; 51(34): 6816–6826. doi:10.1021/bi300870g.

Structures of apo and product-bound human L-asparaginase: Insights into the mechanism of autoproteolysis and substrate hydrolysis

Julian Nomme[1], **Ying Su**[1], **Manfred Konrad**[2], and **Arnon Lavie**[1,*]

[1]Department of Biochemistry and Molecular Genetics, University of Illinois at Chicago, Chicago, USA

[2]Max Planck Institute for Biophysical Chemistry, Goettingen, Germany

Abstract

Asparaginases catalyze the hydrolysis of the amino acid asparagine to aspartate and ammonia. Bacterial asparaginases are used in cancer chemotherapy to deplete asparagine from the blood, since several hematological malignancies depend on extracellular asparagine for growth. To avoid the immune response against the bacterial enzymes it would be beneficial to replace them with human asparaginases. However, unlike the bacterial asparaginases, the human enzymes have a millimolar Km value for asparagine, making them inefficient in depleting the amino acid from blood. To facilitate the development of human variants suitable for therapeutic use, we solved the structure of human L-asparaginase (hASNase3). This asparaginase is an N-terminal nucleophile (Ntn) family member that requires autocleavage between Gly167 and Thr168 to become catalytically competent. For most Ntn-hydrolases this autoproteolytic activation occurs efficiently. In contrast, hASNas3 is relatively stable in its uncleaved state, and this allowed us to observe the structure of the enzyme prior to cleavage. To determine the structure of the cleaved state we exploited our discovery that the free amino acid glycine promotes complete cleavage of hASNase3. Both enzyme states were elucidated in the absence and presence of the product aspartate. Together, these structures provide insight into the conformational changes required for cleavage, and on the precise enzyme-substrate interactions. The new understanding of hASNase3 will serve to guide the design of variants that possess a decreased Km value for asparagine, making the human enzyme a suitable replacement for the bacterial asparaginases in cancer therapy.

Asparaginases are enzymes that catalyze the hydrolysis of the free amino acid asparagine (ASN) into aspartate (ASP) and ammonia. The human genome codes for at least three enzymes that can catalyze this reaction, though the true physiological substrate of these enzymes may not be the free amino acid. One is actually called 60-kDa-lysophospholipase, due to the fact that in addition to asparagine it can hydrolyze lysophospholipids (1). This little-studied enzyme contains an N-terminal domain that is homologous to the *E. coli* Type I and II asparaginases, followed by several ankyrin repeats of unknown function (1, 2). A second human enzyme that can hydrolyze ASN is aspartylglucosaminidase (hAGA). The

*Correspondence should be addressed to A.L. lavie@uic.edu (Tel: 312-355-5029; Fax: 312-355-4535).

Supporting Information Available

Overlay of the cleaved and uncleaved hASNase3 with a zoom of the active site (Figure S1); Overlay of the cleaved and uncleaved hASNase3 with a zoom of the His8-Gly10 loop that change conformation (Figure S2); Sequence alignment of Type III asparaginases (Figure S3); Comparison of hASNase3 to the E. coli and hAGA enzymes (Figure S4); Surface representation of hAGA with the hASNase3 strand A – helix 1 overlaid demonstrating the structural reasons the different substrate specificity (Figure S5). This material is available free of charge via the Internet at http://pubs.acs.org.

main function of this lysosomal enzyme is to remove carbohydrate groups linked to asparagine, as a final step in the degradation of cell surface glycoproteins. Defects in hAGA are the cause of aspartylglucosaminuria (AGU), which is an inborn lysosomal storage disease (3). The third enzyme with asparaginase activity, and the focus of this report, is indeed called L-asparaginase (also known as hASRGL1/ALP(4)/CRASH(5)), despite the fact that it can also hydrolyze isoaspartyl peptide linkages (6), which are a common source of protein damage (7). This enzyme is homologues to the *E. coli* Type III asparaginase, and therefore, we refer to it as human asparaginase 3 (hASNase3).

Type III asparaginases belong to the N-terminal nucleophile (Ntn) family of hydrolases (8). Interestingly, the aspartylglucosaminidase hAGA also belongs to this family. Ntn-enzymes are produced as a single polypeptide that must undergo intramolecular cleavage to attain catalytic activity. The cleavage reaction is an auto-catalytic process, in which the side chain of a threonine/serine/cysteine (depending on the specific Ntn enzyme (9)) residue attacks the carbonyl group of the preceding amino acid to form a covalent intermediate. The intermediate subsequently undergoes hydrolysis to yield the peptide-cleaved enzyme. This type of activation by autoproteolysis is different to that which occurs in proenzymes such as trypsin. In proenzymes, peptide bond cleavage typically functions to displace a short N-terminal inhibitory segment. In contrast, in Ntn-enzymes, cleavage occurs around midway of the peptide sequence, and the resulting two chains, termed α- and β̃ chains, remain intact to form a single functional unit. The purpose of the cleavage reaction is to release the amino group of the Thr/Ser/Cys residue from being involved in peptide bond formation to being N-terminally exposed in the β-chain, which can then attack its substrate. Thus, the Thr/Ser/Cys residue plays dual roles, first in initiating the maturation reaction of the enzyme into its active state, and then in catalyzing hydrolysis of free asparagine or asparagine derivatives. Human ASNase3 differs from most studied Ntn-enzymes by undergoing a very slow self-cleavage reaction. For example, whereas the *E. coli* Type III asparaginase purifies as the fully cleaved form (10), SDS-PAGE of purified recombinant hASNase3 expressed in *E. coli* shows a predominate single band corresponding in size to the uncleaved enzyme, with only weak bands for the lower molecular weight α- and β-chains of the cleaved state. Incubation of hASNase3 in a buffer containing NaCl and Tris/HCl, pH 7.5 increases the proportion of the cleaved state at a very slow rate, as observed by us (manuscript submitted) and others (6). The uncleaved enzyme crystallizes in several salt-containing conditions, such as malonate, citrate, and ammonium sulfate. Diffraction data collected from these crystals show that the extent of protein cleavage (i.e. the peptide bond break between Gly167 and Thr168) is dependent on the age of the crystals, with fresh crystals being uncleaved and older crystals (>90 days) predominantly cleaved. In our earlier work we made the unexpected discovery that the amino acid glycine very selectively accelerates the cleavage reaction (manuscript submitted).

In addition to hydrolyzing ASN and diverse ASN-linked substrates, asparaginases play a prominent role in cancer chemotherapy (11). Bacterial asparaginases, specifically the *E. coli* Type II enzyme (trade name Elspar), its conjugate with polyethylene glycol (PEG), Oncospar, and that from *Erwinia chrysanthemi* (Erwinase) are key agents in inducing remission of acute lymphoblastic leukemia and lymphoblastic lymphoma. Note that these clinically-used asparaginases are not Ntn-enzymes and have a completely different structure to hASNas3 (12); for a discussion of different types of asparaginases, see the recent review by Michalska et al (13). The clinical success of asparaginase therapy is attributed to the rapid and complete depletion of the amino acid ASN in plasma (14). Serum contains a steady-state level of ~50 μM ASN (15). Although ASN is not an essential amino acid, several tissues (thymus, T-cells, etc) depend on extracellular sources of ASN for their metabolic needs. ASN is a crucial amino acid for protein, DNA, and RNA synthesis (16) and its requirement is cell cycle specific for the G1 phase of cell division (17). While a *de*

novo pathway for ASN synthesis exists (via ASN synthetase), many cancer cells such as leukemic cells are dependent on the availability of extracellular ASN. Hence, ASN depletion achieved upon administration of the bacterial asparaginases interferes with the metabolic status of the cancer cell and ultimately results in apoptosis (18).

However, clinical use of these drugs is complicated by an immune response against the bacterial enzymes. Use of the Oncospar version attempts to limit this immunogenicity, based on the observation that foreign proteins covalently linked to PEG may mask immunogenic epitopes. However, eventually enzyme-specific or even PEG-specific antibodies are elicited (19), which cause a variety of adverse effects including hypersensitivity and anaphylactic shock. Moreover, these bacterial asparaginase-specific antibodies inactivate the enzyme and promote its clearance, negating its therapeutic potential. To eliminate the immunogenicity of the enzymes, we propose use of human asparaginases in lieu of bacterial enzymes. However, intrinsically none of the three human asparaginases has the required kinetic property (low μM Km) adequate for replacing bacterial asparaginases. Hence, we commenced the study of hASNase3 with the ultimate goal of engineering a low Km ASN variant suitable for use in humans. As a first step towards this goal, we solved the crystal structures of hASNase3 in various states. Here we present the uncleaved and cleaved enzyme states, either without substrate or in complex with the product L-aspartate. Together these structures reveal details of the substrate-enzyme interactions, inform us on the specific roles of active site residues, and provide insight on the mechanism of autocleavage and ASN hydrolysis.

Materials and Methods

Cloning of human ASNase3

The open reading frame (ORF) of hASNase3 (UniProt Q7L266, also called human asparaginase-like protein 1, hASRGL1, ALP, CRASH) consisting of 927 base pairs, was PCR-amplified using as template cDNA from a human skin and meninges cDNA library (Source Bioscience, UK). NdeI and BamHI sites were incorporated in the oligonucleotides targeting the 5′ and 3′ ORF ends, respectively. The PCR product was gel-purified, digested with NdeI and BamHI-HF (New England Biolabs) and ultimately ligated overnight at 16 °C into pET14b-SUMO vector using T4 DNA ligase. The ligation mixture was used to transform DH5α *E. coli* cells. Positive clones were determined following restriction digestion with NdeI and BamHI-HF, and finally the gene insert was sequenced. The final construct includes an N-terminal 6-histidine tag, followed by SUMO (Small Ubiquitin Modifier; yeast protein Smt3p of 101 residues) tag, which has been proven to improve heterologous protein solubility and stability. For bacterial expression, the *E. coli* BL21(DE3) C41 strain was transformed with the hASNase3 plasmid.

Expression and purification of hASNase3

Two liters of 2YT media was inoculated with a starter culture of *E. coli* BL21(DE3) C41 carrying the hASNase3 plasmid. When the cultures reached an optical density at 600 nm in the range of 0.6–0.8, the temperature was reduced from 37 to 18 °C, 0.5 mM IPTG was added to induce expression, and cells were left to grow overnight. Cells were spun down and then lysed by sonication (Lysis buffer: 50 mM Tris/HCl, pH 7.5, 500 mM NaCl, 10% glycerol, 1% Triton 100, 1 mM PMSF), and the lysate cleared by ultracentrifugation (1 h at 33k rpm). The supernatant was loaded onto a 5 ml His-Trap HP Ni Sepharose column (GE Healthcare), washed with 150 ml of a buffer containing 25 mM Tris/HCl, pH 7.5, 500 mM NaCl and 10 mM imidazole. Further washing was done with a similar buffer that contains 25 mM imidazole. Elution of the protein was accomplished with a buffer containing 250 mM imidazole, with a yield of 290 mg total protein (Bradford assay). At this stage, SUMO protease was added (1:200 weight ratio) to cleave the His-SUMO tag from hASNase3, and

the protein left to dialyze overnight in order to remove the imidazole. The cleaved protein was put back onto the His-Trap column, with hASNase3 coming out in the flow through. After protein concentration to a volume of 5 ml (22 mg/ml), the sample was injected onto a S-200 gel filtration column (GE Healthcare) pre-equilibrated with 25 mM Tris/HCl, pH 7.5, 200 mM NaCl, 2 mM DTT. The protein eluted as two peaks; a minor peak that would correspond to the dimer, and a major peak that would correspond to the monomer. The monomer peak was pooled, concentrated to 38 mg/ml, aliquoted, and stored at −80 °C.

Crystallization of hASNase3

Purified hASNase3 was subject to crystallization condition screening, and crystals of hASNase3 (without added amino acid) were obtained in several conditions with salts as precipitants (e.g. citrate, malonate, ammonium sulfate). Optimization of JCSG+Suite (Qiagen) condition 69 (2.4 M Sodium malonate, pH 7) to 2.2 M malonate resulted in large crystals that diffracted beyond 1.6 Å. For setups, 1 μL of hASNase3 at 38 mg/ml (in 25 mM Tris pH 7.5, 200 mM NaCl, 2 mM DTT) was mixed with 1 μL of the reservoir on a glass cover slip, and left to undergo vapor diffusion using the hanging drop method at 20 °C. Crystals appeared after ~5 days. We also obtained crystals in the JCSG+Suite condition 23 (1.6 M Sodium Citrate) and the Ammonium sulfate Suite (Qiagen) condition 9 (0.2 M Ammonium iodide, 2.2 M Ammonium sulfate).

Crystals used in this study were grown in the malonate condition, except for one substrate-free structure obtained from crystals grown in ammonium sulfate. Electron densities resulting from crystals grown in these three different conditions revealed precipitant molecules occupying the substrate binding site (see below). To solve this precipitant-competition problem for the purpose of obtaining the structure of hASNase3 in complex with L-aspartate (ASP), crystals grown in malonate were transferred to a 2 M aspartate pH 7.5, 20% glycerol solution for 5 min. In order to obtain the fully cleaved structure in complex with ASP, we first transferred crystals to a 2 M glycine solution pH 7.5 for 1 min, and then to the 2 M ASP pH 7.5, 20% glycerol solution for 5 min.

Data collection and structure solution of hASNase3

Diffraction data were collected using the in-house x-ray source (Rigaku RU-200 rotating anode) with a R-Axis IV++ image plate detector. Data were processed using XDS (20). The structure was solved by molecular replacement (Molrep (21) CCP4) using the bacterial asparaginase EcAIII as starting model (PDB entry 2ZAK), and refined with Refmac5 (22). Structure figures were made with PyMol. All crystals were perfectly twinned, with the true space group being $P6_5$ (apparent space group, $P6_522$), and contained two copies of hASNase3 in the asymmetric unit. Data collected on freshly grown crystals showed the uncleaved state of the enzyme, whereas older crystals the cleaved state. In all the crystallization conditions mentioned above, the salt used as precipitant was observed at the enzyme active site. Attempts to soak in the product ASP, even at a concentration of 100 mM, failed to result in density for this amino acid. We interpret this as being due to competition by the precipitant salt. Hence, to obtain the ASP complex, we transferred crystals into a high concentration ASP solution that acted to stabilize the crystals and to provide the source of the amino acid binding at the active site.

Results and Discussion

Cleaved versus uncleaved states of hASNase3

We solved two amino acid-free hASNase3 structures, one from crystals grown with ammonium sulfate as the precipitant (at 2.13 Å resolution) and another from crystals grown in malonate (1.85 Å). Data collection and refinement statistics are presented in Table 1.

Regardless of the precipitant used, the crystals adopted the same space group and unit cell dimensions, contained two molecules in the asymmetric unit, and were invariably twinned. Additionally, in every case we observed a precipitant molecule bound at the active site (see below). This is not surprising due to the similar structural properties of the precipitants and the substrate ASN.

Human ASNase3 is a homodimer, and its structure obtained from crystals grown in ammonium sulfate revealed the uncleaved state of the enzyme in both protomers. We could model several sulfate molecules, with one sulfate at the active site (hence the designation sulfate-complex). Likewise, the structure from the malonate condition contained the predominantly uncleaved state in protomer A (protA; modeled as 75% uncleaved/25% cleaved). In contrast, protomer B (protB) of the malonate-grown crystal was observed to be 100% cleaved. We could model a malonate molecule bound at the active site of protA (hence the designation malonate-complex) but not in protB. Apart from localized structural differences due to cleavage of protB, these substrate-free structures from the different precipitants are basically identical (rmsd 0.27 Å over 529 Cα-atoms). A comparison of all uncleaved protomers discussed here is presented in Fig. S1. Based on the fact that the amino acid-free structure of the malonate complex was of higher resolution, and since it allows us to compare the uncleaved-versus-cleaved state from the same crystal (Fig. 1a), our analysis of the amino acid-free structure is focused on this data set.

The amino acid-free hASNase3 structure is presented as a ribbon diagram of the dimeric asymmetric unit (Fig. 1b). However, it is unclear if this dimer (interface area ~1,800 $Å^2$; PISA server (23)) is indeed the physiological oligomeric state for hASNase3 since the gel filtration elution profile shows a major peak corresponding to the monomer, and only a minor peak corresponding to the dimer. This is similar to the observation made with the homologous glycosylasparaginase from *Flavobacterium meningosepticum*, where only a monomer was observed using gel filtration (24). On the other hand, all known structures of Ntn-enzymes, including the latter one, reveal a similar dimeric arrangement, suggesting that the dimer is physiologically relevant. Since active site residues originate from a single protomer, and since kinetic studies have not observed cooperativity, dimer formation may serve only a stabilizing role. The uncleaved protA of hASNase3 (shown in green, Fig. 1) has a malonate molecule (depicted in magenta, Fig. 1b) at the active site, whereas the active site of the uncleaved protB (shown in dark and light blue representing the α- and β-chains, respectively) is occupied by solvent molecules. The reason for this difference is not clear, and does not seem to be a result of the cleavage status. The determination of cleaved versus uncleaved enzyme state was made based on two criteria: one, the presence or absence of electron density extending in the N-terminal direction from Thr168. In this amino acid-free structure, for protA we could model the preceding Gly167 and the main chain atoms of Leu166 (at 75% occupancy), but not beyond (Fig. 1c and 1d, zoom). In contrast, for protB the electron density did not extend beyond Thr168, and hence it was designated as cleaved. The second criterion was the conformation of Gly9, which we observe for the first time for Ntn-enzymes, to flip depending on the cleavage state of the enzyme (Fig. S2). Interestingly, a glycine at this position is common for Ntn-enzymes (Fig. S3), suggesting that this glycine-enabled peptide flip is important for stabilizing the cleaved state. We discuss the possible function of this region in the section detailing the cleavage mechanism.

Despite the fact that protA was uncleaved, residues spanning His153 and Leu166 lacked clear electron density (Fig. 1c). This observation is consistent with that made with other Ntn-enzymes (25, 26) that even in the uncleaved state (in those cases, requiring mutants devoid of cleavage ability) several residues at the tip of the α-chain cannot be modeled, suggesting that this region is intrinsically disordered. In the cleaved protB we also could only trace the α-chain as far as His153, demonstrating that after cleavage, the most C-

terminal residues of the α-chain (residues 154–167) do not adopt a defined conformation. Whereas the two protomers differ in their cleavage state and in the presence of precipitant molecule bound at the active site, their overall structure is nearly identical, with an rmsd of 0.31 Å over 267 atoms (Fig. 1d). Hence, cleavage does not induce a significant conformational change, with the most pronounced differences between the cleaved and uncleaved enzyme being the positioning of Thr168 (Fig. 1d, zoom), which differs by 0.6 Å (Cα-atom), and the aforementioned conformation of Gly9. In the cleaved state, a water molecule occupies the position previously taken by Gly167. Of course, the most significant aspect of the cleavage is the liberation of the amino group of Thr168, which then becomes the N-terminal residue of the β-chain, and can now participate in catalyzing ASN hydrolysis. To our knowledge this is the first structure of an uncleaved Ntn-enzyme obtained without resorting to mutations that abolish or slow self-cleavage, an accomplishment made possible by the intrinsically slow cleavage rate of hASNase3.

Comparison to *E. coli* Type III asparaginase and hAGA

Both human ASNase3 and AGA are homologs of the *E. coli* Type III asparaginase (Fig. 2a and S3). In terms of overall structure, hASNase3 is highly similar to the *E. coli* Type III asparaginase (25) (rmsd 0.52 Å over 228 atoms; Fig. S4a), yet has significant structural differences with its human homologue AGA (27) (rmsd 1.0 Å over 175 atoms; Fig. S4b), as clearly seen in the overlay of the three enzymes (Fig. 2b). This mirrors the greater sequence homology between hASNase3 and the *E. coli* enzyme (37.5% identity, 64.5% similarity, over 301 residue overlap) compared to that between hASNase3 and hAGA (29.2/60.6% identity/similarity, over 277 residue overlap). The hallmark of these three asparaginases is the presence of three threonine residues at the active site; based on hASNase3 numbering, these are Thr168, Thr186, and Thr219 (Fig. 2a). Also conserved are Arg196 and Asp199 that bind the substrate (see below). Not surprising due to high structural and sequence homology between hASNase3 and *E. coli* Type III asparaginase, these residues occupy identical relative positions in the active site (Fig. 2b, zoom). More remarkable is that these residues also line up exceptionally well with those from the less similar hAGA, demonstrating conserved active site architecture.

Cleaved and uncleaved ASP-complex structures

For insight on how hASNase3 binds its substrate we sought the structure of the enzyme with the product ASP. Hence, preformed crystals were transferred to a solution containing the crystallization mix plus the amino acid (up to 100 mM). However, diffraction data collected on such crystals failed to show electron density for the ASP, instead showing density consistent with the precipitant used in the crystallization. We attribute this to the fact that the precipitant (e.g. malonate, citrate, or ammonium sulfate at over 1.5 M) also binds to the active site, and thus out-competes the soaked-in ASP. To overcome this problem we transferred preformed crystals into a 2 M ASP solution, pH 7.5, with the rationale that such a high amino acid concentration would substitute the precipitant salt in stabilizing the crystal and at the same time provide the ASP that binds at the active site. Indeed, a data set collected on a crystal soaked into ASP (1.75 Å resolution, Table 1) did show a clear electron density for the amino acid, which was present in both protomers.

Recapitulating the observation made with the malonate-complex structure, in this ASP-complex we observed that protA was only partially cleaved (modeled as 50% uncleaved/ 50% cleaved) and protB was fully cleaved, and that the cleaved and partially cleaved protomers have a nearly identical structure (rmsd 0.34 Å on 288 atoms) with differences limited to the cleavage site (Fig. 3a). This structure, designated as the partially cleaved ASP complex, demonstrates that the product ASP, and by analogy the substrate ASN, can bind to the enzyme irrespective of its cleavage status. For the partially cleaved protA, we could

model three residues that precede Thr168, but the residues linking His153 and Asn165 had no interpretable electron density (Fig. 3a, zoom). In the cleaved protomer (protB), we could not build a model beyond His153 of the α-chain. This shows that the presence of product (and presumably of substrate as well) does not induce order to the C-terminal residues of the α-chain (residues 154–167), either in the uncleaved or cleaved state.

This crystal structure allows a direct comparison of ASP binding to the uncleaved and cleaved states of hASNase3 (Fig. 3, zoom) for understanding the essentiality of cleavage for asparaginase activity. The hydrolysis of ASN is thought to commence with the attack of the Thr168 hydroxyl group on the amino acid's side chain carbonyl group. Figure 4 presents a schematic of the hASNase3 asparaginase reaction mechanism, adapted from that previously suggested for hAGA (28). The amino group of Thr168 (free in the cleaved state) acts to activate its hydroxyl group to attack the ASN side chain (panel I), with the negatively charged tetrahedral intermediate being stabilized by the oxyanion hole composed of Thr219 and Gly220 (panel II). Breakdown of the intermediate releases ammonia (panel III) with the amino acid remaining covalently bound to Thr168. The water molecule observed sandwiched between the amino group of Thr168 and the side chain amino group of ASN could act as a proton donor to the leaving NH2 group. Hydrolysis (panel IV) would likely build a very similar tetrahedral intermediate (panel V) to yield the free enzyme and the product ASP (panel VI). In our structures, in both the uncleaved and cleaved states, the Thr168 hydroxyl group is within 2.8–3.1 Å to the ASP side chain carbonyl group. Hence, improper substrate positioning can be ruled out as the reason for the lack of asparaginase activity of the uncleaved enzyme, and supports the catalytic role of the Thr168 amino group as detailed in the reaction schematic.

Product binding to fully cleaved hASNase3

In order to determine the structure of fully cleaved hASNase3 in complex with ASP we took advantage of our discovery that the amino acid glycine promotes the cleavage reaction (manuscript submitted). Hence, a preformed crystal was first transferred into a 2 M glycine solution, pH 7.5, and incubated for ~4 minutes to promote cleavage. Subsequently, the crystal was transferred to a 2 M ASP, pH 7.5 solution, and after a short soak, frozen in liquid nitrogen. Indeed, diffraction data (1.84 Å, Table 1) from this crystal revealed full cleavage of both protomers and the presence of an ASP molecule (Fig. 5a) in each active site of the dimeric enzyme (hence the designation fully cleaved ASP complex). The amino acid is bound at the active site through several polar interactions (Fig. 5b & c): (i) The α-carboxylic moiety forms a bidentate salt bridge with the side chain of Arg196, as well as interacting with the main chain NH-group of Gly222. (ii) The amino moiety of ASP is stabilized by the side chain of Asp199 and by the carbonyl of Gly220. (iii) The carboxylic side chain of ASP is at interacting distance to the side chain of Thr219 and the NH-group of Gly220. Since both of these moieties can function as hydrogen-bond donors, they would interact with the oxygen atom of ASN's side chain, not its amino group. This would orient the side chain such that the leaving group of the reaction, the amino group, is not encumbered by interactions with the enzyme. (iv) Most notable in terms of the reaction mechanism, the ASP carboxylic side chain is at 2.2 Å distance to the hydroxyl of Thr168. In fact, this hydroxyl group is only 2.6 Å from the ASP carboxylate carbon atom (red dashed line, Fig. 5c). The asparaginase reaction is dependent on the free amino group of Thr168, which is thought to be required, directly or via a water molecule (29), to activate the Thr168 hydroxyl group (see proposed mechanism, Fig. 4) (28). Of the water molecules observed closest to the Thr168 amino group (numbered 1, 2, and 3, Fig. 5c), none acts to bridge the amino group and the Thr168 hydroxyl group. Further inspection of this region reveals that nearby water molecules are stabilized by the side chain of Asn62, which is in turn positioned by interactions with Gly187 and Gly188 (Fig. 5d). Hence, in the case of hASNase3, it seems

that the amino group of Thr168 directly activates its hydroxyl group (distance 2.9 Å), and that nearby water molecules, held in position by Asn62, can help to shuttle the proton.

Asn62 is a part of the sodium-binding loop (residues 55 to 65), a feature previously observed previously for this asparaginase family (30), that would anchor its main chain position. Inspection of Ntn-type enzyme sequences shows that Asn62 and the tandem glycine residues following Thr186 (Gly187 and Gly188) are highly conserved (Fig. S3). This supports the model where these conserved residues act to position water molecules near the amino group of Thr168, whose function is to stabilize the protonated amine group once it has abstracted the proton from the Thr168 hydroxyl group (Fig. 4, panels I & II). Interestingly, the homologous asparagine residue in the *E. coli* Type III asparaginase (Asn67) has been implicated in the cleavage reaction (31), suggesting a dual cleavage and asparaginase role for this side chain.

Implication for the auto-cleavage mechanism

In the three crystal structures of hASNase3 analyzed here (for simplicity we omit the sulfate-complex), we observe a total of two protomers in the uncleaved state (protAs of the malonate and partially cleaved ASP-complex) and four protomers in the cleaved state (protBs of the above, plus both protomers of the fully cleaved ASP-complex). What can these structures tell us about the auto-cleavage mechanism? Just as the side chain of the N-terminal threonine of the β-chain is required for ASN hydrolysis, this side chain is also required to initiate the cleavage process. It does this by attacking the carbonyl group of the preceding amino acid, in the case of hASNase3, Gly167. However, in our uncleaved structures the distance between the Thr168 hydroxyl group and the carbonyl carbon atom of Gly167 is too large − 4.0 Å in the case of the uncleaved ASP-complex protomer (Fig. 6a). This suggests that a conformational change is needed prior to this first step of the cleavage reaction. To gain insight as to what this conformational change may be, we analyzed the structures of other asparaginases solved in the uncleaved state. In the case of the glycosylasparaginase from *F. meningosepticum*, this required the use of the W11F mutant (32). In that structure, the distance between the threonine at the scissile position (Thr152) and the carbon atom of the carbonyl group of the preceding residue is only 3.1 Å (Fig. 6b; PDB code 9GAF). Likewise, in the case of the *E. coli* Type III asparaginase, obtaining the structure of the uncleaved state required the mutation of the critical threonine (Thr179) that was replaced by alanine (31). In that structure (Fig. 6c; PDB code 3c17), after first modeling a threonine side chain in place of the alanine (shown in red, Fig. 6c), we measured an analogous distance of 3.2 Å. The central difference between our uncleaved hASNase3 conformation, where the critical distance is too large (Fig. 6a), to that in the uncleaved *F. meningosepticum* and *E. coli* structures, where that distance is more appropriate for a direct attack by the threonine hydroxyl group on the preceding residue's carbonyl group (Fig. 6b and c), is the conformation of the peptide bond that precedes the threonine. Therefore, we suggest that for hASNase3 cleavage to occur, a conformational change in Gly167 is required, such that the distance between the carbonyl group and the Thr168 hydroxyl is shortened. This would necessitate flexibility in this part of the enzyme. Indeed, the conformation of this section differs in the two structures of the uncleaved protomers (Fig. 6d), implying an intrinsic flexibility of the region that would allow for the required conformational change.

One of the few structural consequences of hASNase3 cleavage, from a single polypeptide to the α- and β-chains, is the flip in the conformation of Gly9, a residue in spatial proximity to the cleavage site (double-headed arrow, Fig. 6e). The conformation adopted by Gly9 in the post-cleavage state would be incompatible with the conformation of Gly167 in the pre-cleavage state (Fig. 6e). In fact, the flip-in Gly9 conformation may act to promote the change in conformation of Gly167 to one that brings its carbonyl group closer to Thr168,

and in so doing, promotes the cleavage reaction. In conclusion, our structures suggest that the inherent flexibility of the cleavage region is required for the buildup of a cleavage-competent hASNase3 conformation.

Rationalizing the substrate specificity of hASNase3

Enzymes such as human ASNase3 and AGA, in addition to being able to hydrolyze the free amino acid ASN, show hydrolytic activity with ASN-derivatives. For example, hAGA's main function is to hydrolyze ASN-linked oligosaccharides in the lysosome, and hence its designation as aspartylglucosaminidase. In contrast, hASNase3 does not hydrolyze ASN-linked sugars, but is able to hydrolyze isoaspartyl linkages (6). The shape of the active site cavities would dictate this difference in substrate specificity, prompting us to analyze the geometries of the active site entrance regions.

Common to both enzymes is the orientation of the minimal substrate, the amino acid ASN: the amino acid binds with its α-amino and carboxyl groups oriented towards the center of the protein, and with the side chain pointing out (Fig. 7a–d). Divergence occurs as to the space possible for derivatives to extend from the ASN side chain. In the case of hASNase3, any molecule connected to the ASN side chain would most likely take one path (dotted black line, Fig. 7b), whereas in hAGA, it would take an alternate path (dotted white line, Fig. 7d). These paths are mutually exclusive since structural elements in one occupy the path most likely to be taken by the ASN-derivative in the other. More specifically, residues only present in true asparaginases (such as *E. coli* Type III asparaginase and hASNase3), and missing from aspartylglucosaminidases (such as hAGA), block the path that would be required for the sugar derivative (Figs. S3 and S5). For example, hASNase3 differs from hAGA by having a long linker between β-strand A and α-helix 1 (for secondary structure labeling see Fig. 1b). Modeling of such a long linker (extra 16 residues) in hAGA demonstrates that this linker would block the space most likely to be required by the sugar moiety of an ASN-sugar derivative (Fig. S5). This analysis illuminates the structural reasons behind the different substrate specificities of human ASNase3 and AGA.

Conclusions

Here, we present the crystal structures of amino acid-free and ASP-complexed human asparaginase 3, in both the uncleaved (inactive) and cleaved (active) states. The ASP-complex structures, in addition to supplying a detailed view of the interactions made between the enzyme and the product of the reaction, ASP, suggest that in the cleaved state, a direct interaction between the Thr168 amino and hydroxyl groups takes place. It is this interaction that would activate the Thr168 hydroxyl group for attack on the side chain of the substrate ASN. The slow intrinsic auto-cleavage rate of hASNase3 allowed us to observe the uncleaved state without resorting to cleavage-inactivating mutations. The structures also suggest a role for the conserved N-terminal segment (His8-Gly9) in promoting the cleavage-competent conformation, a feature not noted previously for other members of this enzyme family. Any modifications to hASNase3 done for the purpose of lowering its ASN Km value, to allow it to act as a replacement of bacterial asparaginases in blood cancer therapy, would need to take these aspects into consideration, so as to still permit the essential intramolecular cleavage reaction.

Supplementary Material

Refer to Web version on PubMed Central for supplementary material.

Acknowledgments

This work was supported by a National Institutes of Health grant (R21 CA155424) and the Max Planck Society.

We thank UIC's Research Resources Center and in particular Bernard Santarsiero for assistance with the in-house x-ray equipment. We also thank the three anonymous reviewers for their constructive comments.

Abbreviations

hASNAase3	hASRGL1
Ntn	N-terminal nucleophile
hAGA	human aspartylglucosaminidase

References

1. Sugimoto H, Odani S, Yamashita S. Cloning and expression of cDNA encoding rat liver 60-kDa lysophospholipase containing an asparaginase-like region and ankyrin repeat. J Biol Chem. 1998; 273:12536–12542. [PubMed: 9575212]
2. Menniti M, Iuliano R, Foller M, Sopjani M, Alesutan I, Mariggio S, Nofziger C, Perri AM, Amato R, Blazer-Yost B, Corda D, Lang F, Perrotti N. 60kDa lysophospholipase, a new Sgk1 molecular partner involved in the regulation of ENaC. Cell Physiol Biochem. 2010; 26:587–596. [PubMed: 21063096]
3. Mononen I, Fisher KJ, Kaartinen V, Aronson NN Jr. Aspartylglycosaminuria: protein chemistry and molecular biology of the most common lysosomal storage disorder of glycoprotein degradation. Faseb J. 1993; 7:1247–1256. [PubMed: 8405810]
4. Bush LA, Herr JC, Wolkowicz M, Sherman NE, Shore A, Flickinger CJ. A novel asparaginase-like protein is a sperm autoantigen in rats. Mol Reprod Dev. 2002; 62:233–247. [PubMed: 11984834]
5. Evtimova V, Zeillinger R, Kaul S, Weidle UH. Identification of CRASH, a gene deregulated in gynecological tumors. Int J Oncol. 2004; 24:33–41. [PubMed: 14654938]
6. Cantor JR, Stone EM, Chantranupong L, Georgiou G. The human asparaginase-like protein 1 hASRGL1 is an Ntn hydrolase with beta-aspartyl peptidase activity. Biochemistry. 2009; 48:11026–11031. [PubMed: 19839645]
7. Aswad DW, Paranandi MV, Schurter BT. Isoaspartate in peptides and proteins: formation, significance, and analysis. J Pharm Biomed Anal. 2000; 21:1129–1136. [PubMed: 10708396]
8. Brannigan JA, Dodson G, Duggleby HJ, Moody PC, Smith JL, Tomchick DR, Murzin AG. A protein catalytic framework with an N-terminal nucleophile is capable of self-activation. Nature. 1995; 378:416–419. [PubMed: 7477383]
9. Galperin MY, Koonin EV. Divergence and convergence in enzyme evolution. J Biol Chem. 2012; 287:21–28. [PubMed: 22069324]
10. Borek D, Jaskolski M. Crystallization and preliminary crystallographic studies of a new L-asparaginase encoded by the Escherichia coli genome. Acta Crystallogr D Biol Crystallogr. 2000; 56:1505–1507. [PubMed: 11053866]
11. Verma N, Kumar K, Kaur G, Anand S. L-asparaginase: a promising chemotherapeutic agent. Crit Rev Biotechnol. 2007; 27:45–62. [PubMed: 17364689]
12. Swain AL, Jaskolski M, Housset D, Rao JK, Wlodawer A. Crystal structure of Escherichia coli L-asparaginase, an enzyme used in cancer therapy. Proc Natl Acad Sci U S A. 1993; 90:1474–1478. [PubMed: 8434007]
13. Michalska K, Jaskolski M. Structural aspects of L-asparaginases, their friends and relations. Acta Biochim Pol. 2006; 53:627–640. [PubMed: 17143335]
14. Appel IM, Kazemier KM, Boos J, Lanvers C, Huijmans J, Veerman AJ, van Wering E, den Boer ML, Pieters R. Pharmacokinetic, pharmacodynamic and intracellular effects of PEG-asparaginase in newly diagnosed childhood acute lymphoblastic leukemia: results from a single agent window study. Leukemia. 2008; 22:1665–1679. [PubMed: 18580955]

15. Avramis VI, Tiwari PN. Asparaginase (native ASNase or pegylated ASNase) in the treatment of acute lymphoblastic leukemia. Int J Nanomedicine. 2006; 1:241–254. [PubMed: 17717965]
16. Ellem KA, Fabrizio AM, Jackson L. The dependence of DNA and RNA synthesis on protein synthesis in asparaginase-treated lymphoma cells. Cancer Res. 1970; 30:515–527. [PubMed: 5458976]
17. Gong SS, Basilico C. A mammalian temperature-sensitive mutation affecting G1 progression results from a single amino acid substitution in asparagine synthetase. Nucleic Acids Res. 1990; 18:3509–3513. [PubMed: 1972978]
18. Ueno T, Ohtawa K, Mitsui K, Kodera Y, Hiroto M, Matsushima A, Inada Y, Nishimura H. Cell cycle arrest and apoptosis of leukemia cells induced by L-asparaginase. Leukemia. 1997; 11:1858–1861. [PubMed: 9369418]
19. Armstrong JK, Hempel G, Koling S, Chan LS, Fisher T, Meiselman HJ, Garratty G. Antibody against poly(ethylene glycol) adversely affects PEG-asparaginase therapy in acute lymphoblastic leukemia patients. Cancer. 2007; 110:103–111. [PubMed: 17516438]
20. Kabsch W. Automatic processing of rotation diffraction data from crystals of initially unknown symmetry and cell constants. J Appl Crystallogr. 1993; 24:795–800.
21. Vagin A, Teplyakov A. MOLREP: an automated program for molecular replacement. J Appl Cryst. 1997; 30:1022–1025.
22. Murshudov GN, Vagin AA, Dodson EJ. Refinement of macromolecular structures by the maximum-likelihood method. Acta Crystallogr D Biol Crystallogr. 1997; 53:240–255. [PubMed: 15299926]
23. Krissinel E, Henrick K. Inference of macromolecular assemblies from crystalline state. J Mol Biol. 2007; 372:774–797. [PubMed: 17681537]
24. Xuan J, Tarentino AL, Grimwood BG, Plummer TH Jr, Cui T, Guan C, Van Roey P. Crystal structure of glycosylasparaginase from Flavobacterium meningosepticum. Protein Sci. 1998; 7:774–781. [PubMed: 9541410]
25. Michalska K, Bujacz G, Jaskolski M. Crystal structure of plant asparaginase. J Mol Biol. 2006; 360:105–116. [PubMed: 16725155]
26. Wang Y, Guo HC. Crystallographic snapshot of glycosylasparaginase precursor poised for autoprocessing. J Mol Biol. 2010; 403:120–130. [PubMed: 20800597]
27. Oinonen C, Tikkanen R, Rouvinen J, Peltonen L. Three-dimensional structure of human lysosomal aspartylglucosaminidase. Nat Struct Biol. 1995; 2:1102–1108. [PubMed: 8846222]
28. Tikkanen R, Riikonen A, Oinonen C, Rouvinen R, Peltonen L. Functional analyses of active site residues of human lysosomal aspartylglucosaminidase: implications for catalytic mechanism and autocatalytic activation. Embo J. 1996; 15:2954–2960. [PubMed: 8670796]
29. Guo HC, Xu Q, Buckley D, Guan C. Crystal structures of Flavobacterium glycosylasparaginase. An N-terminal nucleophile hydrolase activated by intramolecular proteolysis. J Biol Chem. 1998; 273:20205–20212. [PubMed: 9685368]
30. Prahl A, Pazgier M, Hejazi M, Lockau W, Lubkowski J. Structure of the isoaspartyl peptidase with L-asparaginase activity from Escherichia coli. Acta Crystallogr D Biol Crystallogr. 2004; 60:1173–1176. [PubMed: 15159592]
31. Michalska K, Hernandez-Santoyo A, Jaskolski M. The mechanism of autocatalytic activation of plant-type L-asparaginases. J Biol Chem. 2008; 283:13388–13397. [PubMed: 18334484]
32. Xu Q, Buckley D, Guan C, Guo HC. Structural insights into the mechanism of intramolecular proteolysis. Cell. 1999; 98:651–661. [PubMed: 10490104]

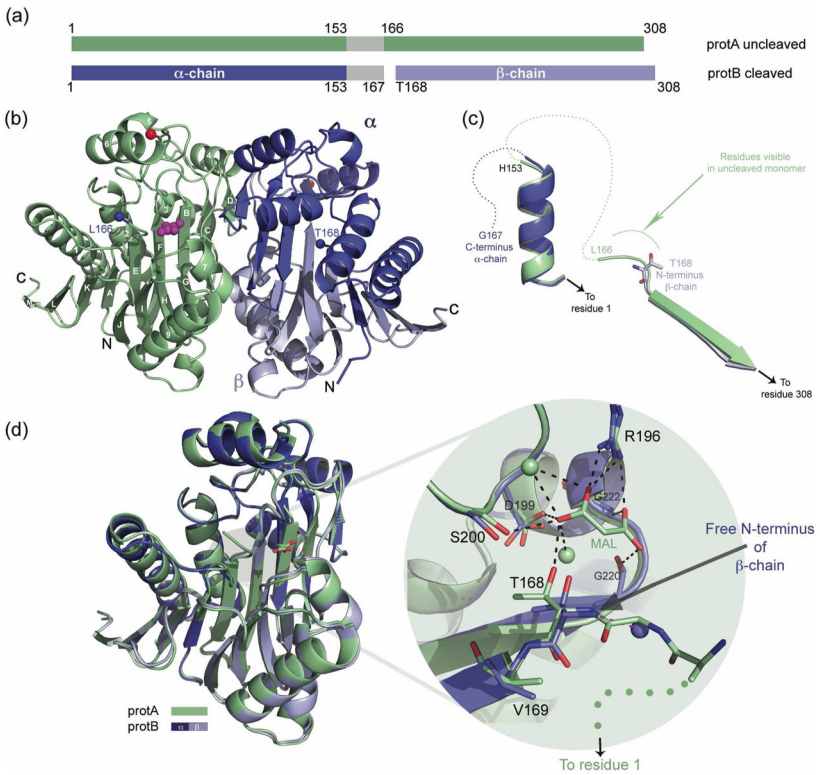

Figure 1. Cleaved versus uncleaved structures of substrate-free hASNase3

(a) schematic representation of hASNase3 as observed in the dimeric asymmetric unit of the malonate complex. The entire uncleaved protomer (protA) is depicted in green color, except for regions lacking interpretable electron density, which are in gray. The cleaved protomer (protB) is illustrated in dark and light blue, representing the α- and β-chains, respectively. (b) Ribbon diagram of the hASNase3 dimer, colored as in (a), with the secondary structure elements annotated. The protA active site-bound malonate is shown in magenta. Red and blue spheres represent the terminal amino acids visible in the flexible H153-T168 loop. (c) Overlay of the uncleaved (protA) and cleaved (protB) protomers, focused on the structural elements spanning the cleavage site. See text for details. (d) Overlay as in (c), depicting the entire molecule, demonstrates that the uncleaved and cleaved conformations are essentially identical. Right panel zooms on the cleavage site. The bound malonate (MAL) is shown in sticks, and black dashed lines represent interactions with the enzyme and solvent (green spheres). Upon cleavage, the space previously occupied by G167 is taken by a water molecule (blue sphere).

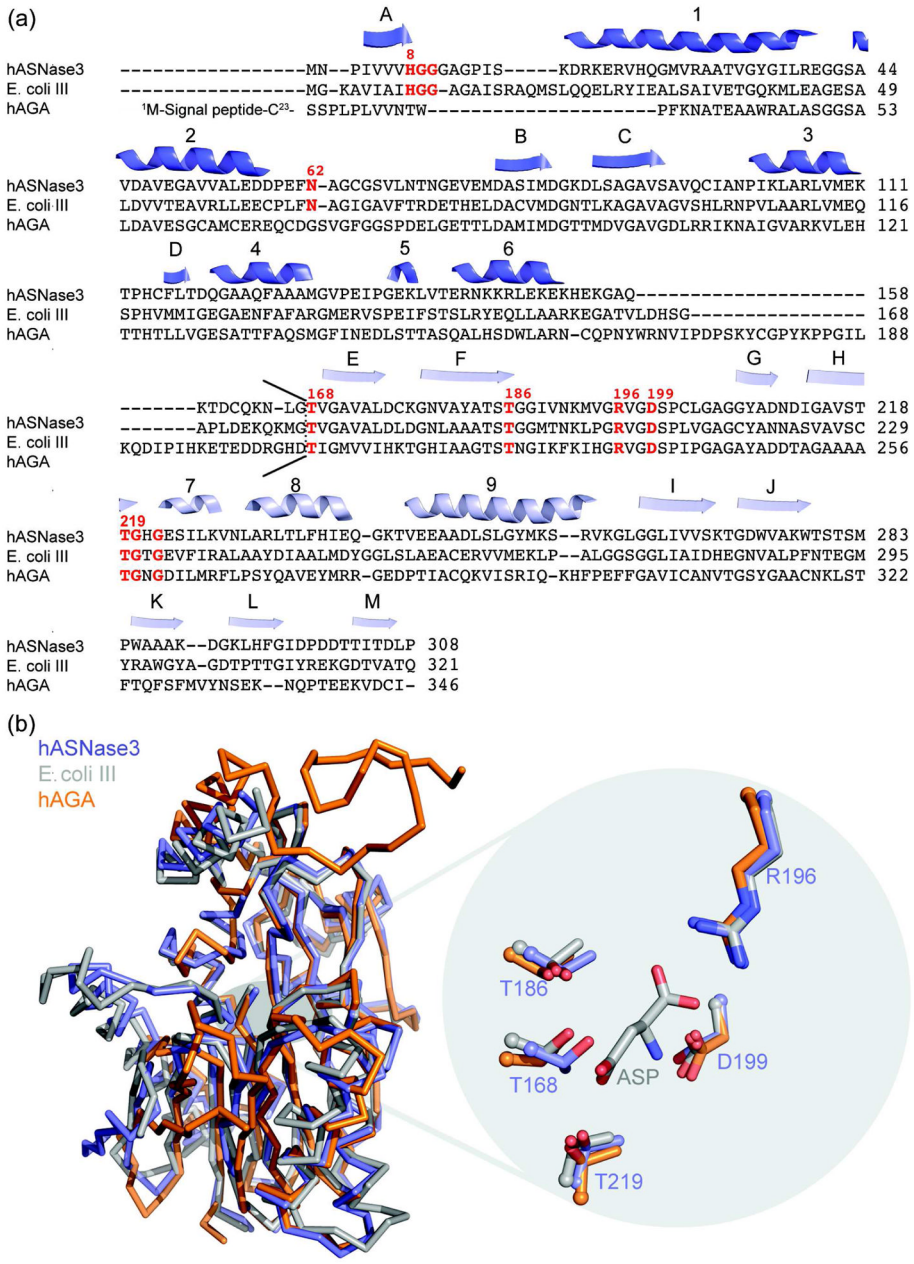

Figure 2. Sequence and structure alignment of hASNase3, *E. coli* Type III, and hAGA

(a) The sequences of hASNase3 (ASGL1_HUMAN), *E. coli* Type III (IAAA_ECOLI) and hAGA (ASPG_HUMAN) are aligned using Clustal W program. The 23 first amino acids corresponding to the hAGA signal peptide are not shown. hASNase3 secondary structure elements are presented and annotated (α- and β-chain in dark and light blue, respectively). Conserved active site residues are shown in red. The cleavage site for these Ntn-enzymes is marked by a black line. (b) Overlay of hASNase3, *E. coli* Type III (pdb code: 2ZAL) and hAGA (pdb code: 1APZ), colored in blue, gray and orange respectively. The right panel zooms on the highly conserved active site threonines and aspartic acid/arginine residues (hASNase3 numbering). Depicted ASP molecule (gray sticks), as seen in the *E. coli* Type III structure.

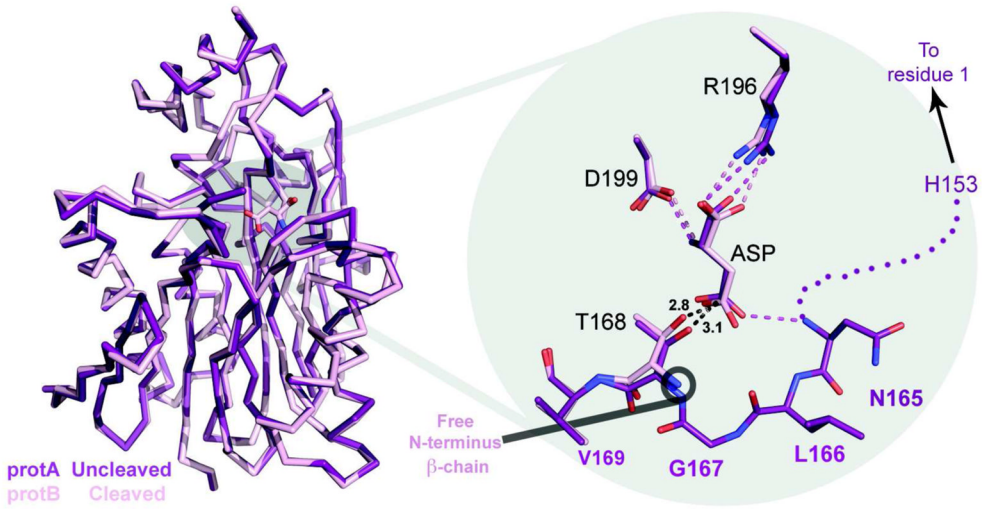

Figure 3. Comparison of the ASP-bound enzyme conformation in the cleaved and uncleaved states

Cα-trace representation of superimposed hASNase3 protA (uncleaved, magenta) and protB (cleaved, pink) as observed in the partially cleaved ASP complex structure. Aspartate (ASP) represented as sticks. Right panel highlights the active site residues binding the ASP (colored dashed lines). Uncleaved-protA residues surrounding T168 are shown, with the dotted line representing residues lacking interpretable electron density. Cleaved-protB residues T168 and V169 are also shown. Note the small change in position of T168 upon cleavage.

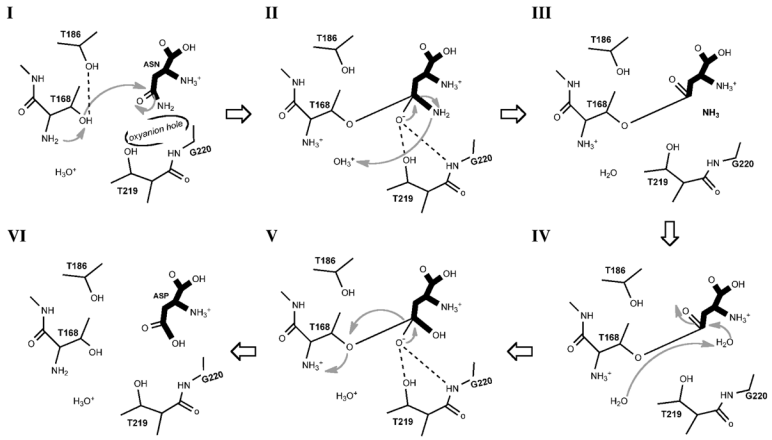

Figure 4. hASNase3 reaction mechanism

In the enzyme's cleaved state, the amino group of Thr168 acts to activate its side chain for attack on the ASN side chain (panel I). The ensuing negative charge of the tetrahedral intermediate is stabilized by the oxyanion hole composed of Thr219 and Gly220 (II). The water molecule flanking the Thr168 amino group and the ASN side chain could act as a proton donor for the leaving group. After release of ammonia (III), a water molecule hydrolyzes the covalent intermediate (IV) via a similar tetrahedral state (V) to yield the product ASP and the free enzyme. Reaction mechanism adapted from Tikkanen et al (28). Experimentally derived distances between ASP and the enzyme are shown in Fig. 5b.

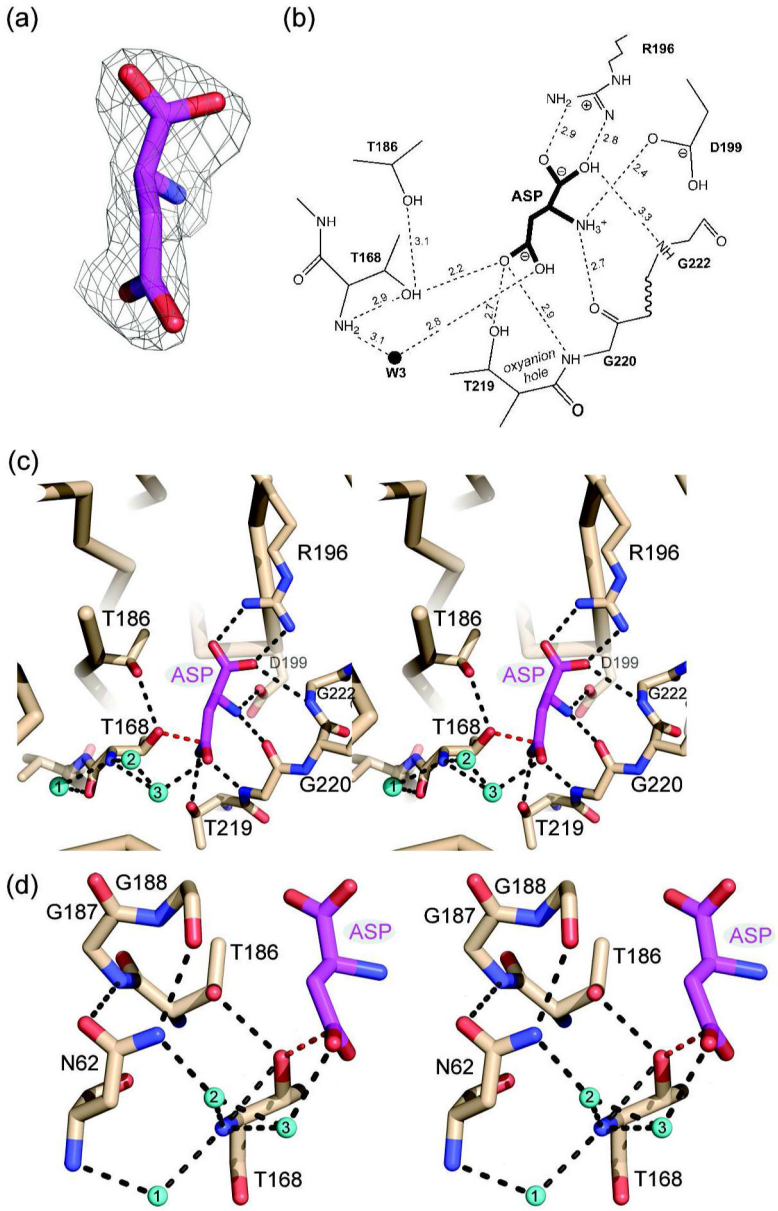

Figure 5. Fully cleaved hASNase3 structure in complex with ASP

(a) ASP 2F_o-F_c omit map. ASP conformation is defined in unbiased electron density that was calculated before the ligand was built in (contour level of 1σ). (b) Schematic representation of ASP bound at the hASNase3 active site. Numbers represent distances in Å. W3 is one of three water molecules in the vicinity of the Thr168 amino group (c) Stereo view of hASNase3 active site from the fully cleaved ASP complex structure (in tan). Black dashed lines indicate interaction with ASP (magenta) interactions and solvent molecules (labeled 1 to 3). The red dashed line shows the distance between Thr168 hydroxyl group and ASP beta-carboxylate carbon atom (2.6 Å). (d) Stereo view of the region around N62 and T168, with interactions denoted by dashed lines. The N62 side chain, positioned by interactions with conserved G187 and G188, acts to stabilize water molecules (labeled 1, 2, and 3) in the vicinity of the Thr168 amino group.

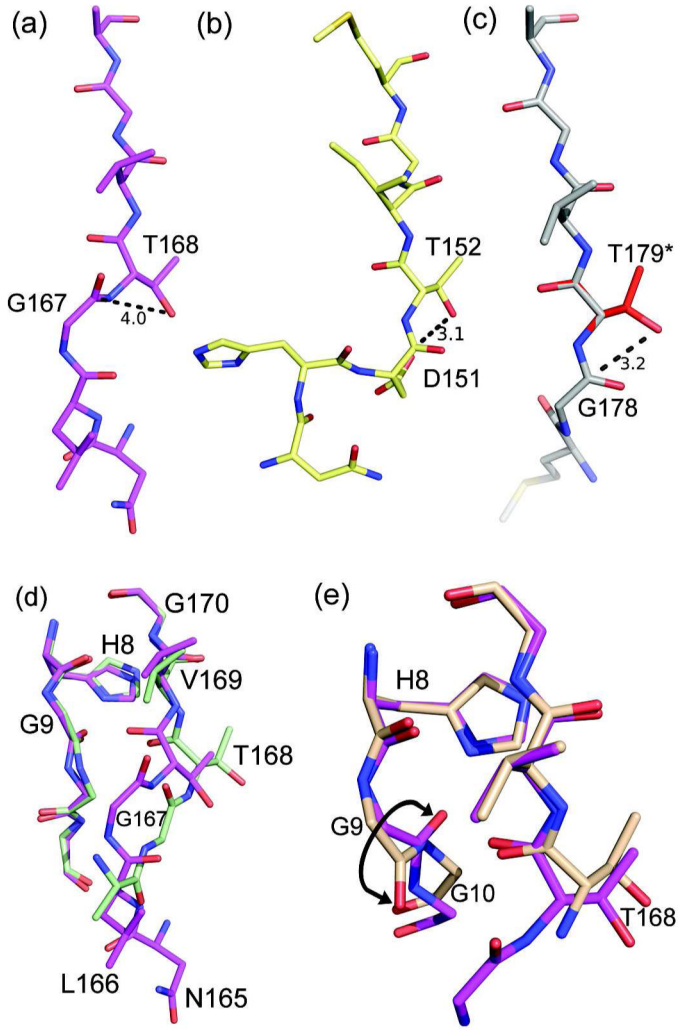

Figure 6. hASNase3 cleavage requires flexibility at the cleavage site

Structural comparison of three mechanistically related asparaginases in their precleaved state. (a) hASNase3 (partially cleaved ASP-complex; uncleaved protA) cleavage site. Distance from Gly167 carbonyl carbon atom to Thr168 hydroxyl group is 4.0 Å. (b) *F. meningosepticum g*lycosylasparaginase (PDB code: 9GAF) cleavage site. Distance from Asp151 carbonyl carbon atom to Thr152 hydroxyl group is 3.1 Å. (c) *E. coli* Type III asparaginase (PDB code: 3C17) T179A mutant cleavage site. T179* indicates a threonine modeled by us at this position. Distance from Gly178 carbonyl carbon atom to T179* hydroxyl group is 3.2 Å. (d) Overlay of the active site of hASNase3 uncleaved protomers from the substrate-free (green) and ASP-bound (magenta) structures. Residues N-terminal to Val169 adopt a slightly different conformation, showing the intrinsic flexibility of this region. (e) hASNase3 fully cleaved protomer (tan) and uncleaved protomer from the partially cleaved (magenta) ASP-bound structures are superimposed. The double-headed arrow indicates the Gly9 flip upon cleavage.

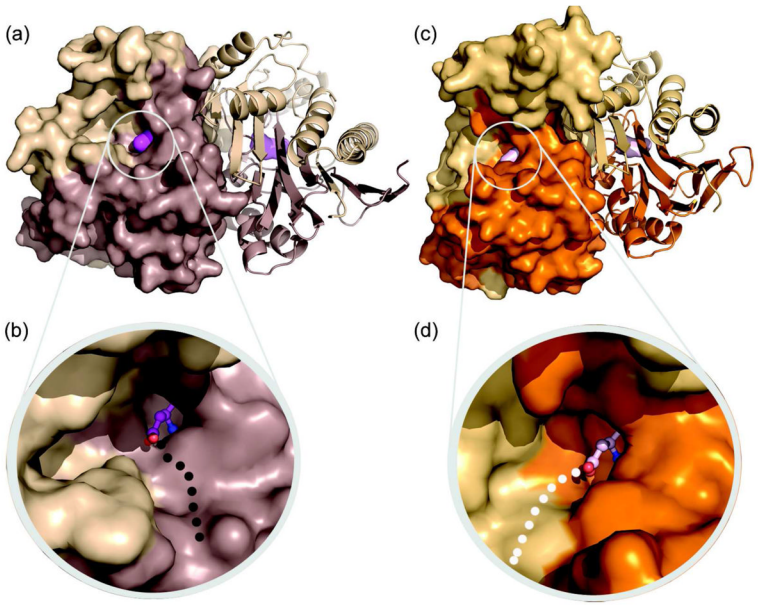

Figure 7. hASNase3 substrate specificity

The different substrate-binding cavities between hASNase3 and hAGA rationalize their distinctive substrate specificities to ASN-derivatives. (a) Dimeric hASNase3 fully cleaved ASP-complex is represented as a surface for protA and ribbon diagram for protB, colored in light and dark shades corresponding to the α- and β-chains, respectively. ASP is shown in magenta. (b) Zoom on the hASNase3 active site entrance. ASP is represented in ball-and-stick mode, and the black dotted line indicates the space available for the ASN derivative moiety, such as a sugar or aspartyl group. (c) Dimeric hAGA ASP-complex (pdb code 1APZ), represented as in (a) using light and dark orange shades for the α- and β-chains. ASP is depicted in pink. (d) Zoom on the hAGA active site entrance. ASP is represented in ball-and-stick mode, and the white dotted line indicates the space available for the ASN derivative moiety, such as a sugar or aspartyl group. Note the difference in positioning of the cavity, and its larger size in hAGA.

Table 1

Data collection and refinement statistics

Complex	Sulfate complex	Malonate complex	Partially cleaved ASP complex	Fully cleaved ASP complex
PDB codes	4GDU	4GDT	4GDV	4GDW
Data collection statistics				
X-ray source and detector	R-AXIS IV ++	R-AXIS IV ++	R-AXIS IV ++	R-AXIS IV ++
Wavelength (Å)	1.5418	1.5418	1.5418	1.5418
Temperature (K)	93	93	93	93
Resolution[a] (Å)	2.13 (2.13–2.25)	1.85 (1.85–1.96)	1.75 (1.75–1.80)	1.84 (1.84–1.96)
Number of Reflections				
Observed	91279	217177	339360	143931
Unique	26285	48285	59545	50184
Completeness (%)	79.4 (53.5)	94.7 (69.5)	99.2 (96.1)	97.4 (88.4)
R_{sym} (%)	6.7 (32.5)	4.7 (24.9)	6.1 (31.4)	3.9 (42.1)
Average I/σ(I)	12.81 (2.89)	18.44 (2.58)	17.35 (2.02)	16.94 (2.10)
Space group	P65	P65	P65	P65
Unit cell (Å): a=b	59.22	59.46	59.50	59.67
c	298.48	298.90	299.50	298.72
Refinement statistics				
Refinement program	REFMAC5	REFMAC5	REFMAC5	REFMAC5
Twinning fraction	0.531	0.506	0.503	0.501
Rcryst (%)	16.9	16.2	16.1	17.1
Rfree (%)	22.3	20.5	19.1	21.6
Resolution range (Å)	51.3–2.13	51.5–1.85	51.5–1.75	51.7–1.84
Protein molecules per a.u.	2	2	2	2
Number of atoms:				
Protein (protA, protB)	2132, 2149	2186, 2172	2196, 2165	2165, 2165
Malonate/SO_4^{2-}	-/13	7/-	-/-	-/-
Aspartate	-	-	2 × 9	2 × 9
Water molecules	212	251	263	259
Na^+	2 × 1	2 × 1	2 × 1	2 × 1
I^-	4	-	-	-
R.m.s. deviation from ideal:				
Bond length (Å)	0.010	0.011	0.010	0.009
Bond angles (°)	1.30	1.28	1.27	1.22
Average B-factors (Å^2)				
Protein (protA, protB)	27.3, 27.2	22.9, 23.4	12.6, 12.9	25.4, 25.5
Malonate/SO_4^{2-}	-/30.1	23.4/-	-/-	-/-
Aspartate	-	-	20.5, 22.1	19.7, 26.5
Water molecules	25.0	24.4	17.5	28.1
Na^+	30.2, 24.6	25.3, 27.5	8.4, 13.2	21.2, 47.5
I^-	51.6	-	-	-

Complex	Sulfate complex	Malonate complex	Partially cleaved ASP complex	Fully cleaved ASP complex
Ramachandran plot (%):				
most favored regions	88.8	89.5	90.8	89.9
additionally allowed regions	10.3	9.9	8.6	9.7
generously allowed regions	0.2	0.2	0.4	0.0
disallowed regions	0.6	0.4	0.4	0.4

[a]Last shell in parentheses